forests

MDPI

Article

Assessment of the Impact of Industry-Related Air Emission of Arsenic in the Soils of Forest Ecosystems

Mikhail V. Shabanov [1], Maksim S. Marichev [1], Tatiana M. Minkina [2], Saglara S. Mandzhieva [2,*] and Dina G. Nevidomskaya [2]

[1] Department of Soil Science and Agrochemistry, Saint-Petersburg State Agrarian University, Saint-Petersburg 196601, Russia
[2] Academy of Biology and Biotechnology, Southern Federal University, Rostov-on-Don 344006, Russia
* Correspondence: msaglara@mail.ru

Abstract: The soils of forest ecosystems are often affected by the industrial activity of mining and metallurgical enterprises, and insufficiently investigated for the content of pollutants due to enterprise emissions. Some pollutants, such as arsenic, are transported over long distances by these emissions. To analyze this connection, the present study was conducted on the eastern slope of Mount Yurma, the Southern Urals, Russia, to determine the content of arsenic in the soils of mountain forest areas in the impact zone of the copper smelter (Karabash). The physical and chemical parameters, total content of arsenic, mineralogical composition of silt, and concentration of arsenic in the silty fraction in soils located at different altitudes were determined using atomic absorption spectroscopy (AAS) and X-ray diffraction (XRD) techniques. The soils under study are physico-chemically and chemically acidic in the upper horizons with a pH of 3.26 to 4.05. The carbon of organic matter decreases with depth from 7.98 to 0.06%. Exchangeable Ca and Mg cations in the range of 2.6–8.6 mg-eq per 100 g of soil were determined. The mineralogical composition of the silty fraction consists mainly of quartz and aluminosilicates. Following an analysis of the arsenic content in the aboveground leaf litter, the bioconcentration factor (BCF) was calculated. Arsenic exceeding Clarke concentrations was recorded. In all upper soil horizons, concentrations of total arsenic exceeded background values by 3.7–5.2 times, with maximum values in the horizons A—25.3 mg/kg, in the horizons O—64.4 mg/kg. The obtained BCF > 1 data points to the biological arsenic accumulation by plants and, as a result, its input into the soil via industrial emissions from the smelter. It was found that the silty fraction plays a special role in the accumulation of arsenic in the studied soils. Accumulation of arsenic occurred mainly due to the secondary minerals of Ca and Mg. Differences in the accumulation of arsenic in the forest litter depending on the plant association were noted. The obtained results could serve as a guideline for monitoring the areas around the enterprise and enhancing the understanding of pollutants' distribution in the soils of remote areas and mountain landscapes.

Keywords: Leptosols; arsenic; soil formation in mountains; pollution; forest ecosystems

Citation: Shabanov, M.V.; Marichev, M.S.; Minkina, T.M.; Mandzhieva, S.S.; Nevidomskaya, D.G. Assessment of the Impact of Industry-Related Air Emission of Arsenic in the Soils of Forest Ecosystems. *Forests* **2023**, *14*, 632. https://doi.org/10.3390/f14030632

Academic Editor: Xiankai Lu

Received: 22 February 2023
Revised: 15 March 2023
Accepted: 17 March 2023
Published: 20 March 2023

1. Introduction

One of the main and most toxic pollutants from mining activities is arsenic, listed after Hg, Pb, and Cd as the fourth most toxic metal [1,2]. Arsenic is widely distributed in the biological cycle through the uptake by farm animals of plant products containing high concentrations of arsenic [3], possesses the high ability to migrate [4,5] and spreads over significant distances by air mass transfer, which was studied in detail: in the mountainous regions of China [6,7], in agricultural landscapes in France and Germany [8], in the rice fields of China, India, and Thailand [9], on the coasts of England [10], and in industrial areas of Spain [11], Canada [12], and Brazil [13].

Arsenic is an isomorphic element in copper-pyrite ores. Once it enters the soil, it can be converted to different states. Depending on the changes in redox conditions, it may convert to As (III) As (IV) [14,15], and play an important role in its migration. Most strongly, in soils, arsenic is retained by oxides of Fe and Mn [16,17]. Organic matter can provide high sorption of As [18–20]. Despite landscape zone conditions, where mining enterprises are concentrated, the formation of anomalous zones with high concentrations of pollutants inevitably occurs, which leads to changes in the ecological and geochemical characteristics of the depositing media [21–24]. Among all the varieties of the skeletal part of the soil, the silty fraction is more represented by secondary minerals, which in turn act as sorbents of arsenic. However, in different climatic conditions, especially in dynamically changing mountainous terrain, the processes occurring in the soil can vary greatly.

The study of the relationship between forest vegetation and soils in conjugated landscapes is of particular interest, especially in mountain ecosystems where the soil-vegetation layer is formed under the influence of a complex of factors. Industrial air emissions from nonferrous metallurgy enterprises contribute significantly to the disturbance of forest ecosystems, resulting in geochemical contrast at various distances from the copper smelter. Mountain soils inevitably act as a barrier to the spread of pollution and concentrate a number of pollutants. The territory of the Ural region of Russia is intensively affected by the technological activities of the mining industry, and their impact on fragile forest mountain ecosystems is increasing every year and poses a threat to human health and the overall environmental safety of the territories. In this regard, Mount Yurma is one of the brightest objects for studying the effect of industrial air emissions from the copper smelter on the soils of mountainous forest areas. The copper smelter is located in the Chelyabinsk region of the Southern Urals, in the town Karabash, 15 km west of Mount Yurma.

The blister copper smelter has been in operation for over 110 years. In the first half of the 20th century, due to a lack of technology to clean up production wastes and waste gases, the areas around the mill were subjected to heavy streams of pollutants. As a result, the landscapes around the copper smelter have changed and become devoid of vegetation, in some areas for up to 10 km. Therefore, much attention has been paid to the problem of pollution in this region. Multiple monitorings of pollution of atmospheric air [25], soils [26,27], bottom sediments [22], water bodies, and vegetation [28] have been conducted in the immediate vicinity of the enterprise and in the area of intensive technogenic load. The ecosystems and soils located in the distance received almost no attention. To analyze this connection, the main purpose of the present study was to identify the impact of industrial air emissions from the copper smelter on the arsenic accumulation in the soils of mountainous forest areas. The silt fraction of soils, acting as the main barrier to arsenic migration, was considered as a priority objective.

2. Materials and Methods

2.1. The Object of Study

The object of the study was soils of the eastern slope of the Yurma mountain range (Chelyabinsk region, Southern Urals, Russian Federation) (Figure 1). The absolute height of the Yurma mountain peak is approximately. 1003 m. The mountain range is composed of crystalline rocks: miascites, quartzites, and syenites.

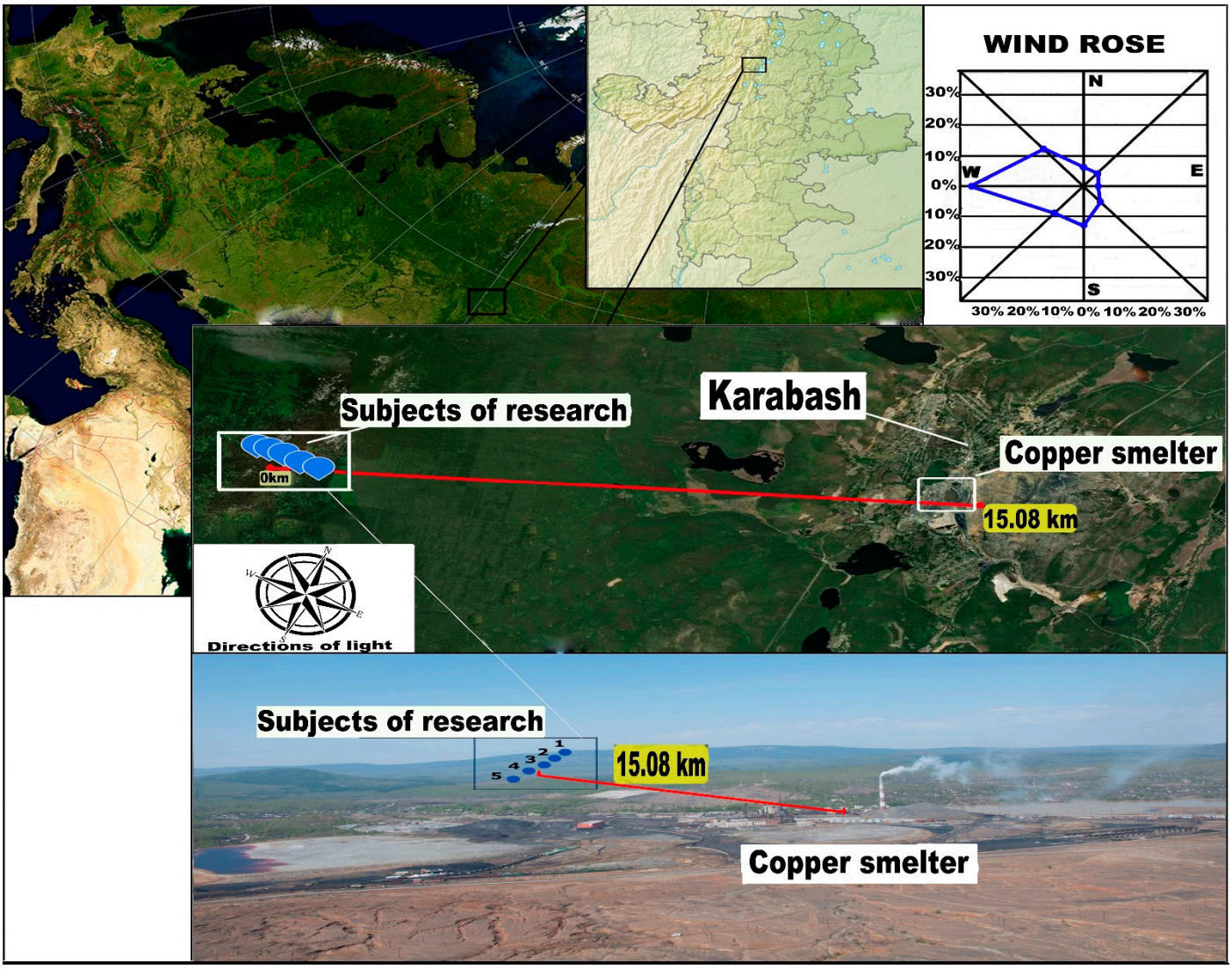

Figure 1. Sampling sites, eastern slope of Yurma Mountain. 1-5 – the location of the soil profile.

The climate features are long, cold winters with a steady snow cover and short, warm (sometimes hot) summers. For the mountain forest zone, the number of windy days per year is 140. The most precipitation falls at Zlatoust (624 mm) and Asha (761 mm). The summer months are the wettest, with about half of the annual amount of precipitation. The winter period accounts for no more than 25% of the annual amount. There is a clearly expressed vertical vegetation zonation: mountain-forest (up to heights of 800–850 m), a zone of subalpine crooked forests (850–900 m), and a zone of alpine deserts represented by quartzite remnants (above 900 m) [29].

2.2. The Methods of Research

Sampling was conducted on the eastern slope of Yurma mountain, 15 km west of the Karabash copper smelter. During the work, 5 points were planned at which soil and plant samples were taken at different heights: 824, 762, 727, 670, and 549 m. Sampling points were laid along the mountain slope on the approach to the mill at a distance of 0.5 km from each other. The height interval between the two points was 35–60 m. Soil sampling was done based on ISO 18400–104 [30]. Soil samples were taken from the vertical soil profile at an interval of 10 cm from the upper boundary to the bedrock by following a standard sampling mechanism. The selected soil samples were delivered to the laboratory in plastic bags. Each bag was labeled, with information about the coordinates of the

sampling site and characteristics of the sample. During the field study, the soils on the eastern slope were classified as Hyperskeletic Leptosols cambic (located on the slope) and Luvisols albic (located at the foot of the slope) in accordance with the World Reference Base for Soil Resources [31].

2.2.1. Soil Properties, Description

The western slope of the Yurma mountain range is a trans-elluvial landscape with various plant communities. The main soil cover is Hyperskeletic Leptosols cambic, with Luvisols albic covering the foothills. These soils cover thin sandy loam and medium-loam sediments, which are underlain by dense rocks (quartzites) at a depth of 30–40 cm. Four soil profiles were used to study the morphological structure, physical and chemical properties of Hyperskeletic Leptosols cambic.

Soil profile 1 is located at 824 m above sea level (ASL) in a fern-raspberry spruce forest (Figure 2). Soil profile structure: forest litter O (0–2 cm)—A (2–9 cm)—B (9–24 cm)—R (24–40 cm). Under slightly decomposed peaty litter, a humus horizon is formed, up to 9 cm thick, dark gray (7.5YR 4/3), sandy loam. The illuvial horizon is ochre-colored (10YR 4/4) and sandy loam. Below, there is a weakly weathered parent rock, represented by quartzite eluvium.

Soil profile 2 is made at 762 m ASL in fern-leaved mountain ash. Soil profile structure: O (0–7 cm)—A (7–16 cm)—B (16–31 cm)—R (>31 cm). The main morphological difference is associated with a more powerful organogenic horizon. Under the forest litter, there is the humus horizon, grayish (7.5YR 4/2); below is the illuvial horizon, light loamy, ochreous (10YR 4/4). At 30 cm depth, eluvo-deluvium quartzite rocks represent the bedrock.

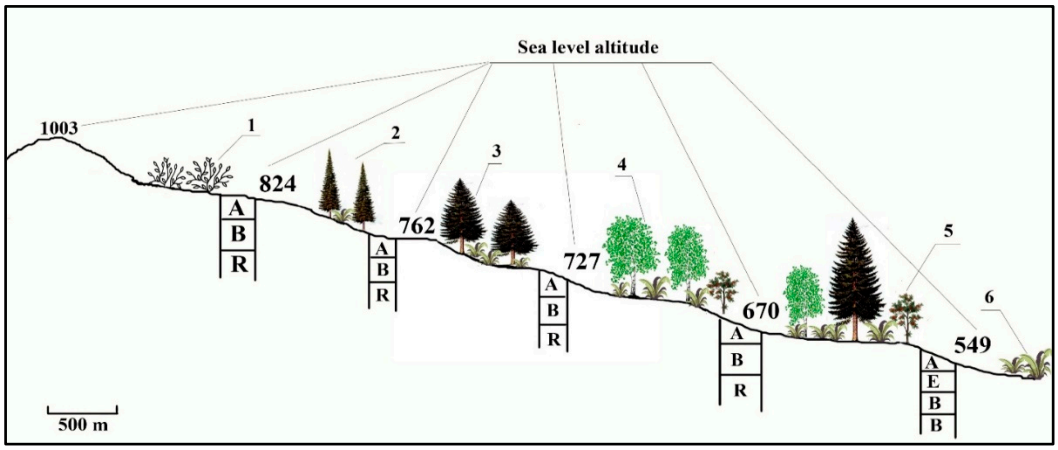

Figure 2. Schematic of the sampling location on the eastern slope of Mount Yurma. 1—dwarf stand; 2—firs; 3—spruce; 4—birch; 5—mountain ash; 6—mixed grass.

Soil profile 3 is located at 727 m ASL in the Crimson Birch Forest. The soil profile is divided into four sections: O (0–7 cm)—A (7–16 cm)—B (16–30 cm)—R (>30 cm). It has an identical morphological structure to the soil profile 2.

Soil profile 4 is located at 670 m ASL in a wood sorrel spruce forest. The soil profile structure is divided into four sections: O (0–3 cm)—A (3–19 cm)—B (19–32 cm)—R (>32 cm). The thin forest litter and medium-loam composition of the illuvial horizon distinguish this section.

Soil profile 5 was plotted at 470 m ASL, in the foothill zone. Soil profile structure: O (0–3 cm)—A (3–23 cm)—E (28–48 cm)—B (48–60 cm). Beneath the forest litter is a thick ochre-gray humus horizon (10 YR 4/3) of light loamy granulometric composition. The eluvial horizon is brownish gray (7.5 YR 4/3), medium loamy, and located at a depth of 28 cm. The illuvial horizon is orange (7.5 YR 6/6), medium-loam.

2.2.2. Soils

In the selected soil samples were determined: the content of carbon of organic matter; actual and potential acidity of soils; exchangeable cations Ca^{2+}, Mg^{2+}, H^{+}, Al^{3+}; granulometric composition; the total content of arsenic; and separately, the content of arsenic in the silty particles of the soil.

Before the laboratory analysis, soil sample preparation was carried out. The selected soils were naturally dried to air-dry state. Subsequently, the soil was crushed in a porcelain mortar and sieved through a sieve of 1 mm diameter.

The soil particle size distribution was performed according to ISO 13317–2 [32]. The pH in a 1:5 soil/water suspension was measured using a glass electrode according to ISO 10390:2005 [33]. Total organic carbon (C_{org}) content was determined by sulfochromic oxidation according to ISO 14235:1998 [34]. The exchangeable cations Ca^{2+} and Mg^{2+} were determined using a hexamine cobalt trichloride solution (ISO 23470:2018 [35]), hydrolytic acidity of the soil (ISO 14254:2018 [36]), exchangeable hydrogen, and aluminum (ISO 14388–3:2014 [37]).

In order to prepare extracts to determine total arsenic, 2.0 g of air-dry soil was poured with concentrated nitric acid, followed by sulfuric acid, and then heated to a temperature of 150–180 °C for 20–30 min. The quantitative content of arsenic in the resulting extracts was measured by atomic absorption spectroscopy (Shimadzu AA-7000) in accordance with ISO 20280:2007 [38].

To extract the silt fraction (soil particles ≤ 0.001), distilled water is added to a cylinder with soil that has passed through a 0.25-mm sieve so that the water column above the bottom of the glass is at least 15–20 cm. The suspension is thoroughly mixed and left to separate the soil particles by sedimentation. After the large particles have been deposited, a silt particle suspension in water is taken for further work. The sedimentation time of particles in a liquid column 7 cm high at a known suspension temperature is calculated using the Stokes formula (as per Equation (1)).

$$V = \frac{2g(d_2 - d_1)}{\mu} \quad (1)$$

where V—sedimentation rate of spherical particles in cm/s; g—acceleration of gravity equal to 981 cm/s^2; d_2—average density of mineral particles; d_1—density of water at a given temperature; r—the particle radius in cm; μ—viscosity of water (in Pa) at a given temperature.

At a suspension temperature of about 20 °C, the time ranges from 21 h and 45 min up to 24 h. After the estimated time has elapsed, the top layer of the soil suspension, which contains only particles of the silt fraction, is drained using a siphon. The samples of the silt fraction were deposited by centrifugation at a speed of 3000 rpm. After being deposited, the clay fraction was dried at room temperature, which is 20 °C. The arsenic content in the obtained fractions was determined [38] and mineralogical composition was determined by X-ray diffraction (XRD) using Cu-Kα radiation and a crystal monochromator. Radiographs were taken at the 2θ values from 2° to 80° at a scan rate of 2°/min [39].

2.2.3. Plants

As an assay for arsenic content of above-ground plant debris was collected. The collection was carried out in autumn on a plot of 1 m^2 at the site of the future soil transect and soil sampling. The collected plant material was stored in tissue bags and immediately transported to the laboratory for analysis. The plants were washed with distilled water, dried at 60 °C, crushed, and sent for analysis. A detailed description of the phytocenotic composition of the studied plots of the plant fallout collection site is presented in Table 1.

Table 1. Characteristics of the sites selected at Mount Yurma.

Soil Type/Soil-Forming Rock	Absolute Height, m	Plant Association	Main Canopy Height, m	Canopy Layer	Shrub Layer	Grass Layer	Moss-Lichen Layer
Mountain forest zone							
Hyperskeletic Leptosols cambic/Quartzite eluvium	824	Fern-raspberry-spruce	10–15	*Picea obovara* L., *Abies sibirica*	*Rubus idaeus*	*Dryopteris filix-mas*, *Milium Effusum* L., *Anemone nemorosa*	*Hypnum imponens*
Hyperskeletic Leptosols cambic/Quartzite eluvium	762	Mountain ash-fern	8–10	*Picea obovara* L., *Abies sibirica*, *Sórbus aucupária*, *Betula pendula*	*Rubus idaeus*	*Dryopteris filix-mas*, *Milium effusum* L.	*Hypnum imponens*
Hyperskeletic Leptosols cambic/Quartzite eluvium	727	Birch-raspberry	10–15	*Betula pendula*, *Abies sibirica*, *Sórbus aucupária*	*Rubus idaeus*	*Dryopteris filix-mas*, *Milium effusum* L.), *Oxalis acetosella* L.	-
Hyperskeletic Leptosols cambic/Quartzite eluvium	670	Wood sorrel-spruce	15–20	*Betula pendula*, *Sórbus aucupária*, *Abies sibirica*	*Rubus idaeus*	*Dryopteris filix-mas*, *Milium effusum* L.	-
Piedmont area							
Luvisols Albic/eluvo-deluvium of metamorphic rocks	479	Meadow grass mix	-	-	-	*Geranium sylvaticum*, *Poa pratensis*, *Dactylis glomerata*, *Filipendula ulmaria*, *Angelica tomentosa*	-

To determine arsenic in plants, the crushed plant sample was subjected to a mixture of concentrated hydrochloric and nitric acids in a ratio of 1:1. It was heated with the gradual addition of hydrogen peroxide. The mixture was boiled for 2 h. The quantitative content of arsenic in the obtained extracts was measured by atomic absorption spectroscopy (Shimadzu AA-7000).

To obtain additional information on the arsenic accumulation in plants, we calculated the bioconcentration coefficient *BCF* (as per Equation (2)) [40].

$$BCF = C_p / C_s \quad (2)$$

where *Cp* and *Cs* are concentrations of the element in plants and soil samples.

To calculate this coefficient, fresh above-ground leaf litter was collected during the autumn. The results obtained were compared to the values of total arsenic in the upper soil horizons [41].

Statistical analysis of measured soil and plant parameters was performed using Microsoft Excel 2017.

3. Results and Discussion

3.1. Physico-Chemical Parameters of Soils

Coarse fractions (fine sand up to 55.4% and coarse dust up to 38.8%) dominate in the profiles of all studied soils, and the content of physical clay increases in the lower part of the slope (up to 47.65%) (Table 2). The slight increase in the total content of all fine-earth fractions from top to bottom along the profile indicates the same intensity of physical and chemical weathering in the formation of the loose eluvium layer [42].

Table 2. Granulometric composition of soils on the eastern slope of Mount Yurma.

Horizon	Depth, cm	Fraction Size, mm						
		1–0.25	0.25–0.05	0.05–0.01	0.01–0.005	0.005–0.001	<0.001	<0.01
		Fraction Proportion, %						
Soil profile 1. Hyperskeletic Leptosols cambic								
A	2–9	25.90 ± 0.02	43.21 ± 0.05	20.30 ± 0.02	8.34 ± 0.04	2.93 ± 0.01	2.82 ± 0.01	14.09 ± 0.01
B	9–24	24.15 ± 0.03	17.05 ± 0.04	38.80 ± 0.03	3.82 ± 0.01	12.65 ± 0.03	3.53 ± 0.02	20.00 ± 0.02

R	24–40	22.45 ± 0.04	14.03 ± 0.01	34.41 ± 0.04	6.74 ± 0.02	15.88 ± 0.05	6.76 ± 0.01	29.38 ± 0.02
Soil profile 2. Hyperskeletic Leptosols cambic								
A	7–16	25.29 ± 0.02	34.19 ± 0.01	14.45 ± 0.02	8.52 ± 0.02	12.26 ± 0.02	2.29 ± 0.01	23.07 ± 0.02
B	16–31	19.12 ± 0.03	22.38 ± 0.02	38.79 ± 0.05	4.12 ± 0.01	11.77 ± 0.05	3.82 ± 0.01	19.71 ± 0.01
R	>31	20.03 ± 0.01	36.47 ± 0.03	9.39 ± 0.01	20.88 ± 0.02	8.82 ± 0.01	4.41 ± 0.02	34.11 ± 0.03
Soil profile 3. Hyperskeletic Leptosols cambic								
A	7–16	38.69 ± 0.02	26.31 ± 0.04	10.42 ± 0.05	7.65 ± 0.01	3.82 ± 0.01	10.47 ± 0.02	21.94 ± 0.01
B	16–30	23.20 ± 0.01	19.18 ± 0.01	28.23 ± 0.02	10.00 ± 0.05	12.35 ± 0.05	7.04 ± 0.01	29.39 ± 0.05
R	>30	26.10 ± 0.02	19.46 ± 0.02	24.12 ± 0.01	12.94 ± 0.01	11.17 ± 0.03	8.24 ± 0.01	32.35 ± 0.04
Soil profile 4. Hyperskeletic Leptosols cambic								
A	3–19	22.50 ± 0.03	15.10 ± 0.01	21.22 ± 0.02	12.06 ± 0.03	21.24 ± 0.04	7.88 ± 0.02	41.18 ± 0.02
B	19–32	18.72 ± 0.01	21.87 ± 0.02	25.29 ± 0.03	11.76 ± 0.04	11.77 ± 0.02	10.59 ± 0.01	34.12 ± 0.01
R	32–50	22.52 ± 0.04	21.01 ± 0.06	25.35 ± 0.04	10.53 ± 0.02	16.47 ± 0.02	4.12 ± 0.01	31.12 ± 0.04
Soil profile 5. Luvisols albic								
A	3–23	33.58 ± 0.02	23.42 ± 0.04	12.35 ± 0.01	4.12 ± 0.01	13.59 ± 0.02	12.94 ± 0.03	30.65 ± 0.04
E	23–28	30.04 ± 0.01	24.67 ± 0.02	14.70 ± 0.03	2.36 ± 0.02	15.88 ± 0.01	12.35 ± 0.02	30.59 ± 0.05
B	28–48	25.45 ± 0.01	13.37 ± 0.02	13.53 ± 0.04	7.65 ± 0.03	14.71 ± 0.02	25.29 ± 0.02	47.65 ± 0.04
B	48–60	20.44 ± 0.02	55.44 ± 0.05	1.18 ± 0.01	0.59 ± 0.01	1.17 ± 0.01	21.18 ± 0.01	22.94 ± 0.03

The distribution of the silt fraction along the profile is uniform. The parent rock and middle part of the profile are enriched in silt. The insignificant content in the upper horizons is associated with more intense weathering processes. The increase in silt in the lower soil horizons is explained by the occurrence of eluvial-illuvial processes [43].

Organic carbon content in the soils of Mount Yurma in the forest litter is significantly higher (9.5%–8.21%) than in the mineral horizons. The intra-profile distribution consists of a gradual decrease in the profile in all soils under study. A distinctive feature of the composition of Hyperskeletic organic matter is its "coarse" nature—the presence of incompletely humified plant residues in its composition.

In the soils in the mineral horizons, the organic carbon content ranges from 2.3% to 7.98%. It should be noted that its content is relatively high in the R horizon (Table 3), except for Luvisols. Under different plant communities, the carbon content of organic matter in the 0–10 cm layer of soils slightly decreases. It is obviously connected with the change in plant community type and nature of plant residues, and as a consequence, the intensity of humification processes changes, which was also described in the study [44]. The authors indicate a significant change in the stability of soil organic matter under changing external conditions, including the composition of vegetation.

Table 3. Physical and chemical properties of soils on the eastern slope of Mount Yurma.

Horizon	Depth, cm	pH_{KCl}	pH_{H2O}	C Organic Matter, %	Hr	Ca^{2+}	Mg^{2+}	H^{+}	Al^{3+}
					mg-eq Per 100 g of Soil				
Soil profile 1. Hyperskeletic Leptosols cambic									
O	0–2	-	-	8.21 ± 0.04	84.50 ± 0.02	7.35 ± 0.06	12.76 ± 0.06	-	-
A	2–9	3.26 ± 0.01	3.95 ± 0.02	7.98 ± 0.04	22.10 ± 0.10	2.60 ± 0.05	0.80 ± 0.02	0.85 ± 0.01	3.75 ± 0.02
B	9–24	3.61 ± 0.02	4.35 ± 0.01	7.31 ± 0.05	14.74 ± 0.12	2.18 ± 0.02	0.83 ± 0.02	0.64 ± 0.02	2.93 ± 0.02
R	24–40	3.75 ± 0.02	4.45 ± 0.02	6.11 ± 0.06	13.28 ± 0.11	2.05 ± 0.01	0.82 ± 0.01	0.52 ± 0.01	3.22 ± 0.02
Soil profile 2. Hyperskeletic Leptosols cambic									
O	0–7	-	-	10.55 ± 0.07	58.30 ± 0.13	8.58 ± 0.04	6.09 ± 0.03	-	-
A	7–16	3.51 ± 0.01	4.69 ± 0.02	5.54 ± 0.06	13.13 ± 0.08	4.85 ± 0.04	0.99 ± 0.01	0.50 ± 0.01	5.33 ± 0.02
B	16–31	3.55 ± 0.02	5.08 ± 0.04	5.23 ± 0.05	11.23 ± 0.09	3.51 ± 0.03	2.60 ± 0.04	0.38 ± 0.02	4.56 ± 0.01
R	>31	3.66 ± 0.03	4.89 ± 0.02	3.11 ± 0.04	11.67 ± 0.09	3.70 ± 0.02	0.57 ± 0.01	0.15 ± 0.01	5.25 ± 0.02
Soil profile 3. Hyperskeletic Leptosols cambic									

O	0–7	-	-	6.00 ± 0.07	37.90 ± 0.15	12.90 ± 0.06	4.82 ± 0.04	-	-
A	7–16	3.71 ± 0.03	4.87 ± 0.03	4.20 ± 0.05	12.29 ± 0.08	4.41 ± 0.02	1.11 ± 0.02	0.30 ± 0.02	2.83 ± 0.02
B	16–30	3.77 ± 0.02	5.00 ± 0.01	3.79 ± 0.02	10.65 ± 0.09	3.20 ± 0.01	1.12 ± 0.02	0.23 ± 0.01	3.08 ± 0.01
R	>30	3.81 ± 0.01	5.06 ± 0.03	2.44 ± 0.01	10.75 ± 0.08	3.69 ± 0.03	1.20 ± 0.01	0.58 ± 0.01	2.48 ± 0.01
Soil profile 4. Hyperskeletic Leptosols cambic									
O	0–3	-	-	7.25 ± 0.06	37.15 ± 0.10	10.45 ± 0.05	12.47 ± 0.06	-	-
A	3–19	3.96 ± 0.02	5.19 ± 0.03	5.78 ± 0.02	11.24 ± 0.11	4.74 ± 0.04	3.51 ± 0.05	0.90 ± 0.04	1.15 ± 0.01
B	19–32	3.76 ± 0.02	5.02 ± 0.03	3.87 ± 0.06	14.65 ± 0.08	3.34 ± 0.01	0.86 ± 0.01	0.28 ± 0.01	2.68 ± 0.02
R	32–50	3.83 ± 0.01	5.04 ± 0.03	2.59 ± 0.01	11.53 ± 0.08	1.32 ± 0.01	2.19 ± 0.05	0.38 ± 0.03	3.18 ± 0.01
Soil profile 5. Luvisols albic									
O	0–3	-	-	9.50 ± 0.02	11.75 ± 0.11	13.65 ± 0.07	6.10 ± 0.06	-	-
A	3–23	4.05 ± 0.03	5.24 ± 0.02	5.60 ± 0.03	12.11 ± 0.09	3.80 ± 0.02	9.50 ± 0.04	0.75 ± 0.04	0.72 ± 0.01
E	23–28	4.06 ± 0.02	5.60 ± 0.01	2.30 ± 0.06	8.43 ± 0.05	3.80 ± 0.03	3.80 ± 0.05	0.55 ± 0.02	0.55 ± 0.02
B	28–48	4.01 ± 0.02	5.38 ± 0.02	0.93 ± 0.04	6.12 ± 0.05	3.51 ± 0.02	4.29 ± 0.04	0.83 ± 0.01	0.48 ± 0.02
B	48–60	3.93 ± 0.01	5.25 ± 0.02	0.06 ± 0.04	6.12 ± 0.07	2.70 ± 0.02	6.50 ± 0.02	0.48 ± 0.02	1.13 ± 0.03

During chemical analysis, the obtained values of pH_{H2O} of Hyperskeletic ranged from 3.95 to 5.19, and pH_{KCl} varied from 3.26 to 4.06. The soils under study demonstrated a strongly acidic reaction to the medium, decreasing with depth (Table 3). The pH_{KCl} value was 3.26 units in the A horizon under the spruce-fern-raspberry community and 3.75 units in the R horizon. In the soil beneath the mountain ash-fern community, the medium reaction was characterized as strongly acidic (pH_{KCl} 3.51–3.66). This pattern is caused by a change in the type of vegetation. The tree layer is dominated by more broadleaf species and, to a lesser extent, coniferous ones; a similar pattern of changes in soil acidity was characterized in the other studies [45].

A similar trend has also been revealed in the soils under the birch-raspberry and wood sorrel-spruce communities, where the reaction of the medium is characterized as strongly acidic. The pH_{KCl} value varies from 3.71–3.96 in the upper part of the profile and 3.81 to 3.83 in the lower part (Table 3). Hydrolytic acidity decreases down the profile, which is associated with a decrease in organic carbon content, which is also reflected in other studies of 91 areas of plant communities with pH measurements, and they found a correlation between changes in soil pH and changes in vegetation type [46]. The changes are more related to the features of the rhizosphere to control the moisture and composition of soil air.

The soils of the middle part of the slope demonstrate the least change in values of hydrolytic acidity with their minimum values: 13.13–11.23 mg-eq/100 g of soil at an altitude of 762 m; the content of exchangeable hydrogen ions being 0.5–0.15 mg-eq/100 g soil; the content of aluminum being 5.33–5.25 mg-eq/100 g of soil. It has been found that Ca predominates in the composition of exchangeable cations in all genetic horizons of soils, while Mg is of subordinate importance, except for Luvisols, where Mg dominates within the horizon, which seems to be due to a change in soil-forming rocks enriched in Mg.

The intra-profile distribution is characterized by the largest amount of absorbed Ca and Mg cations found in the upper part of the profile at a depth of 0–15 cm. This amount varies within: Ca^{2+} from 1.32 to 13.65 meq/100 g of soil; Mg^{2+} from 0.57 to 12.76 mg-eq/100 g of soil (Table 3), which is caused by a change in the type of vegetation and an increase in biological accumulation. The studies conducted by Bhardwaj et al. [47] indicate a close relationship of exchangeable Ca and Mg cations with soil organic carbon and the content of plant residues. The exchangeable cations actively influence the activity of soil microorganisms and control the dynamics of organic matter carbon accumulation.

3.2. Mineralogical Composition of the Silt Fraction

The following minerals are present in the silt fraction in the considered soils: quartz (SiO_2), muscovite ($KAl[AlSi_3O_{10}](OH)_2$), lizardite ($Mg_5[(OH)_8|Si_4O_{10}]$), clinochlor ($Mg_6[Si_4O_{10}](OH)_8$), vertumnite ($Ca_4Al_4Si_4O_6(OH)_{24} * 3H_2O$), rutile ($TiO_2$), and calcite occurs in a single case (Table 4).

Table 4. Mineralogical composition of the silt fraction of soils on the western slope of Yurma Mountain, %.

Horizon	Depth of Sampling, cm	Quartz SiO_2	Calcite	Rutile TiO_2	Muscovite $KAl[AlSi_3O_{10}](OH)_2$	Lizardite $Mg_5[(OH)_8\|Si_4O_{10}]$	Clinochor $Mg_6[Si_4O_{10}](OH)_8$	Vertumnite $Ca_4Al_4Si_4O_6(OH)_{24}$ $3H_2O$
Soil profile 1. Hyperskeletic Leptosols cambic								
O	0–2	-	-	-	-	-	-	-
A	2–9	40.40 ± 0.21	-	-	54.20 ± 0.32	-	5.35 ± 0.21	-
B	9–24	47.90 ± 0.32	-	-	47.2 ± 0.45	-	4.76 ± 0.12	-
R	24–40	45.10 ± 0.50	-	-	44.4 ± 0.21	-	10.90 ± 0.32	-
Soil profile 2. Hyperskeletic Leptosols cambic								
O	0–7	-	-	-	-	-	-	-
A	7–16	38.90 ± 0.42	2.06 ± 0.12	0.73 ± 0.11	45.30 ± 0.21	-	12.90 ± 0.14	-
B	16–31	41.00 ± 0.41	-	-	44.00 ± 0.24	-	14.90 ± 0.14	-
R	>31	42.00 ± 0.55	-	0.39 ± 0.10	45.00 ± 0.12	-	12.50 ± 0.13	-
Soil profile 3. Hyperskeletic Leptosols cambic								
O	0–7	-	-	-	-	-	-	-
A	7–16	44.00 ± 0.61	-	0.83 ± 0.10	43.30 ± 0.32	-	11.60 ± 0.24	-
B	16–30	40.30 ± 0.55	-	0.76 ± 0.05	46.80 ± 0.14	-	12.00 ± 0.25	-
R	>30	43.10 ± 0.45	-	-	42.50 ± 0.24	-	14.20 ± 0.12	-
Soil profile 4. Hyperskeletic Leptosols cambic								
O	0–3	-	-	-	-	-	-	-
A	3–19	39.20 ± 0.12	-	-	49.10 ± 0.21	-	11.60 ± 0.12	-
B	19–32	39.90 ± 0.21	-	0.37 ± 0.04	46.40 ± 0.24	-	13.20 ± 0.14	-
R	32–50	37.70 ± 0.23	-	0.35 ± 0.02	50.60 ± 0.12	-	11.20 ± 0.15	-
Soil profile 5. Luvisols albic								
O	0–3	-	-	-	-	-	-	-
A	3–23	30.20 ± 0.32	-	0.56 ± 0.06	43.20 ± 0.32	25.90 ± 0.24	-	-
E	23–28	30.20 ± 0.32	-	0.56 ± 0.04	43.20 ± 0.15	25.90 ± 0.32	-	-
B	28–48	7.08 ± 0.12	-	-	38.70 ± 0.16	43.40 ± 0.14	-	10.60 ± 0.21
B	48–60	6.38 ± 0.11	-	-	42.80 ± 0.32	44.00 ± 0.31	-	6.73 ± 0.21

The most common and stable among silt minerals are primary minerals such as quartz and muscovite, the content of the former in the studied soils varies across the profile from 6.38 to 44.0%, and the latter from 38.7 to 54.2%. Quartz in silt has been found in all studied soils. In gray-humus (A) horizons under birch-fern-raspberry, spruce-lichen, and mixed grass–barnyard grass communities, the quartz content is increased to values of 30.2%–44.0%. In the soils under the spruce-fern-raspberry and fern-mountain ash communities, on the other hand, the upper part is depleted in quartz while the lower one is enriched. Unlike other minerals, quartz is the most resistant to dissolving in acids excreted into the soil by plants. The most susceptible to change is chloritized mineral structures; therefore, an increased amount of quartz was observed in communities where the most

active destruction of secondary minerals takes place under the influence of plant exudates and accompanying soil biota. The detailed processes of influence of vegetation and soil biota, on the processes of weathering of minerals in the soil were described [48]. In the horizons where these processes do not occur, there is a low quartz content (6.38% in the illuvial horizon of luvisols albic) and an increased amount of secondary minerals were noted. The low solubility of quartz and relatively high solubility of layered silicates are also noted in soils of supergene zones [49]. The studies affect the ionic-molecular level and the mechanisms of direct and indirect influence of plants, biota, and environmental conditions on the weathering of soil minerals.

Mica group minerals are represented by muscovite. This mineral possesses relative chemical stability, and in all investigated soils, is uniformly distributed along a profile. A sufficiently high muscovite content in the soils under study indicates its high resistance to both specific and non-specific organic acids. In studies by Russian scientists, the formation of organo-mineral films on the mica surface in organogenic horizons emphasized the processes of biofilm formation contributing to weathering on the surface of mica minerals that are located in the ectomycorrhizosphere [50,51].

Muscovite resists weathering more than many other aluminosilicates. Its crystal lattice contains aluminum in addition to potassium; therefore, such structures are difficult to transform and degrade and, consequently, slow the release of potassium. As can be seen from the XRD analysis (Table 4), the upper part of the soil profiles is more enriched muscovite than the middle and lower ones. Total chemical composition shows a reverse pattern of distribution, with potassium enrichment of the middle and lower parts of soil profiles.

Secondary minerals are represented by clinochlore (a kind of magnesium chlorite), whose content varies from 4.76 to 14.9%. Clinochlor is found in lithozems, with the exception of luvisols albic. Its distribution along the profile is peculiar; the general pattern is that the minimum occurs in the upper part of the profile [50]. The content of clinochlore in the soil increases with decreasing altitude and acidity (Table 3); however, it is completely absent at the foot of the slope. This pattern can be explained by the low acid resistance of chlorine group minerals. These minerals demonstrate the fastest buffer capacity with respect to an acid in soils since acidic solutions cause aluminum interlayers to dissolve. It was indicated the dissolution rate of aluminosilicates depends on changes in the pH of the environment [51]. The dissolution rate increased with decreasing pH. The dissolution process proceeded in stages. In the first stage, proton complexes were formed, which destabilized the metal-oxygen bonds. The second stage was in breaking the Si-O and Al-O bonds. Considering this, its content in luvisols albic soil, whose pH is the highest among the studied soils (pH_{H2O} 5.24), should be the highest, but clinochlorine is completely absent in this soil, probably due to a pronounced eluvial process [51].

Serpentinites, as well as chlorites (provided their compositions and properties are similar), can form mixed-layer minerals. It is also assumed that magnesian chlorites (including clinochlore) are magnesian-aluminum serpentinites, an intermediate stage between lizardite and amesite [51], whereas chlorites are mixed-layer minerals of serpentinites and amesite. Given these facts, it is reasonable to assume that clinochlor would clinochlor react with lizardite to form avertumnite [50].

Sokolova [49] described the mechanism of mixed-layer chlorites and noted the possibility of chlorite degradation occurring during brucite layer dissolution with subsequent migration of dissolution products. The destruction of trioctahedral chlorites is most likely to follow the same way as the dissolution of micas in the biotite-phlogopite series. The major rearrangement of the crystal lattice of micas and chlorites can occur only under acidic conditions that provide excess hydrogen ions and a flushing regime. As a result, in cases where lizardite and clinochlore interact in the acidic reaction of the medium and flushing water regime, a similar process occurs.

Rutile is located mainly in the upper and middle parts of the soil; it has not been found under the spruce-linden-fern community. Rutile is TiO_2 found in igneous rocks; its

absence in the upper part of some soils (Table 4) can only be explained by its presence in the parent rock and physical transport.

Lizardite and vertumnit are found only in the soil under the mixed–barnyard grass community. The minimum amount of lizardite is observed in the upper part and the maximum in the lower part of the profile. Vertumnitis is found only in the lower part. Lizardite accumulation in the foothill area along with its absence in the soils on the mountain slope can be correlated with the change in the parent rock from eluvium and eluvium-deluvium of metamorphic rocks on the slope to eluvium and eluvium-deluvium of serpentinite rocks. Lizardite is capable of accumulating iron oxides; Mg^{2+} in the structure of serpentinites can be isomorphically replaced by Fe^{2} and Fe^{3+} [52].

Vertumnite is a mineral belonging to the group of layered silicates with a complex tetrahedral structure. It was discovered at the end of the last century, and therefore has been poorly studied, especially in soils. A single occurrence of calcite in Hyperskeletic Leptosols cambic can be accounted for by a single calcite outcrop in the parent rock [41,53,54].

3.3. Arsenic in Soils

The silt soil fraction, which has a high absorption capacity and reflects the absorption of elements by the mineral part, can serve as an indicator of pollutants' accumulation during ecological and geochemical monitoring. Thus, the studies of silty and clayey fractions of soils showed the high adsorption capacity of silty fractions of soils. [55].

The detailed analysis of changes in the physical and chemical parameters of soils on the eastern slope of Mount Yurma revealed changes in the acid-base properties of soils that indicate the influence of technological factors. Since the soils under study are located in natural landscapes far from populated areas (the nearest city is Karabash, more than 10 km to the east), one of the sources of pollutant input into the studied soils was industrial emissions from the Karabash copper smelter (KCS). Chemical analysis of the silt fraction in the soils under study revealed high concentrations of arsenic (Table 5).

Table 5. Arsenic content in the objects under study.

Horizon	Depth of Sampling, cm	As in Soil, mg/kg	As mg/Silt Weight	BCF
Soil profile 1. Hyperskeletic Leptosols cambic				
O	0–2	64.40 ± 0.25	-	3.12
A	2–9	20.60 ± 0.24	1.81 ± 0.05	
B	9–24	3.19 ± 0.12	1.15 ± 0.06	
R	24–40	2.81 ± 0.11	0.19 ± 0.02	
Soil profile 2. Hyperskeletic Leptosols cambic				
O	0–7	36.85 ± 0.13	-	1.45
A	7–16	25.30 ± 0.15	4.40 ± 0.04	
B	16–31	6.77 ± 0.11	0.87 ± 0.01	
R	>31	5.35 ± 0.18	1.27 ± 0.02	
Soil profile 3. Hyperskeletic Leptosols cambic				
O	0–7	17.20 ± 0.21	-	0.81
A	7–16	21.40 ± 0.14	6.28 ± 0.03	
B	16–30	5.45 ± 0.21	2.93 ± 0.02	
R	>30	4.32 ± 0.14	1.81 ± 0.01	
Soil profile 4. Hyperskeletic Leptosols cambic				
O	0–3	49.75 ± 0.13	-	2.64
A	3–19	18.80 ± 0.11	5.72 ± 0.06	
B	19–32	6.31 ± 0.08	2.72 ± 0.03	
R	32–50	5.29 ± 0.09	1.26 ± 0.04	

Soil profile 5. Luvisols albic				
O	0–3	13.50 ± 0.14	-	0.65
A	3–23	20.60 ± 0.15	18.71 ± 0.04	
E	23–28	7.56 ± 0.11	3.84 ± 0.02	
B	28–48	12.56 ± 0.11	1.51 ± 0.01	
B	48–60	11.77 ± 0.08	0.00	

Thus, at an altitude of 824 m, Hyperskeletic Leptosols cambic exhibit the illuvial-accumulative type of the intra-profile differentiation of arsenic in the silt fraction. There is a tendency of arsenic accumulation in the middle part of the profile. The obtained data correlation coefficient (Table 6) recorded a close relationship with exchangeable Ca and Mg cations, at the correlation coefficient 0.96–0.98. The close relationship is probably associated with the transfer of arsenic in gas dust emissions in the form of Ca and Mg silicate minerals. The mineralogical and elemental analysis of suspended particles was carried out and the content of some heavy metals and As was found to be high [56]. The high concentrations of heavy metals and As emission and distribution characteristics were also shown from coal-fired power station [57].

Table 6. Correlation coefficient between physicochemical properties and total arsenic concentration in soils.

	pH_{H2O}	**pH_{KCl}**	**C Organic Matter**	**Ca^{2+}**	**Mg^{2+}**	**Fraction Size, <0.001 mm**
Soil profile 1	−0.99	−0.97	0.73	0.98	0.96	−0.65
Soil profile 2	−0.84	−0.75	0.89	0.92	0.70	−0.98
Soil profile 3	−0.97	−0.94	0.68	0.49	0.39	0.91
Soil profile 4	0.98	0.91	0.91	0.98	0.99	0.16
Soil profile 5	−0.76	0.13	0.42	0.05	0.91	−0.14

In Hyperskeletic Leptosols cambic down the slope at an altitude of 762 m, a sharp increase in arsenic has been recorded in the silt fraction of the humus-eluvial horizon. This fact can only indicate the input of arsenic and its accumulation in the humus-eluvial horizon with forest litter, provided the soil under study and the soil located higher along the slope have equivalent characteristics such as mineralogical composition, sesquioxides, pH, and organic carbon content. In this soil, the increase in total arsenic content is regulated by both Ca and Mg minerals and organic matter, which is confirmed by a close correlation of 0.89 (Table 6). Consequently, sorption with humus matter increases. These changes occur due to a change in the type of vegetation and because of changes in the humus state of soils; the arsenic accumulation by different types of vegetation, and the behavior of the element in the soil. The results of their work confirm the heterogeneity of As accumulation in the root layer and under different vegetation, which is associated with the processes of leaching in the soil and different bio-absorption capacity [58,59].

Down the slope, significant succession and the presence of broad-leaved vegetation result in a constant seasonal input of arsenic absorbed by the leaves. Therefore, the mineral part of the soil is replenished with arsenic that comes with the decomposition products of leaf litter, which has also been noted in studies of the accumulation of As by different tree species. They concluded that As accumulation in a greater proportion falls on leaves compared to other vegetative organs of trees [60]. As a result of arsenic accumulation in the upper part of the soil with plant residues, arsenic migrates and is distributed within the soil profile according to the progressive-accumulative type [60].

In Hyperskeletic Leptosols cambic at an altitude of 727 m, a distinctive feature is observed in the intra-profile distribution of arsenic in the silty soil particles. Even a higher arsenic concentration in the humus-elluvial horizon compared to the soil higher up the slope is related to a change in vegetation to the broad-leaved and more abundant grass

cover and, as a consequence, high phytoaccumulation of arsenic. The increased pollutant concentration in silty fractions of the parent rock is most likely due to sesquioxide migration and sorption. Additionally, an increase in the percentage of clinochlore acts as an active sorbent. This mineral will adsorb arsenic compounds not only by exchange sorption but also by specific chemisorption. Chemisorption by this group of minerals has been comprehensively studied [61–63]. The clay minerals sorb As, and the rate of sorption directly depends on the acidity of soils. As a result, accumulative-elluvial-illuvial differentiation is formed in these soils. Correlation analysis confirms a close relationship between sludge fraction and arsenic content in the soil, at coefficient value of 0.91 (Table 6). Plants play one of the key roles in the migration of arsenic in soils. At this site, when changing the type of vegetation to broad-leaved with grass cover, the BCF coefficient decreases sharply, which is most likely caused by a smaller share of biological absorption of arsenic compounds by this type of vegetation compared to conifers. Along with this, we noted heterogeneous content of As in the forest litter of different compositions [64].

Down the slope at an altitude of 670 m, in Hyperskeletic Leptosols cambic, arsenic concentrations in the silt fraction of soils decrease again compared with the previous site by 8 times in the upper part of the profile and 34 times in the parent rock. This decline is probably due to lower arsenic input with leaf phytomass due to the change of vegetation to coniferous wood, which was observed at an altitude of 824 m. The pollutant distribution in the silty fraction is accumulative-elluvial-illuvial. Again, with the appearance of the coniferous type of vegetation, the BCF coefficient increases. In the O horizon, the values of the total content of arsenic are more than 2 times higher in comparison with the profile of soil No. 3. In soil No. 4, as in the profiles of soils No. 1 and 2, the main limiting indicators in the intraprofile differentiation of arsenic are exchangeable calcium and magnesium cations, in conjunction with changes in environmental acidity, as evidenced by the close correlation (Table 6) as well as in the studies by several scientists. It was proved the influence of exchangeable calcium cations on its migration ability in the soil by conducting an experiment on introducing calcium carbonates and calcium-magnesium composite [65,66]. In both cases, the results coincided; an increase in the proportion of exchange ions increased sorption of arsenic in the soil and decreased its migration.

In Luvisols Albic, located at an altitude of 549 m, arsenic concentrations increase in the silt fraction of the gray-humus horizon. This area is the least susceptible to the impact of technogenic flows due to the more distant mass transfer of arsenic. Nevertheless, the trend in arsenic accumulation only in the upper gray-humus and eluvial horizons indicates the technogenic impact. The intraspecific distribution of arsenic in the silt fraction is regressive-accumulative, and among the total content of arsenic progressive-elluvial-illuvial. A marked decrease in arsenic concentrations in the E horizon is associated with the destruction and removal of minerals due to the eluvial process. The calculated values of correlation coefficients indicate the lack of relationship between changes in the total concentration of arsenic and pH_{KCl}, sludge fraction and exchangeable calcium cations. Arsenic contamination of forest soils and methods of remediation of soils from As note the high role of biota in the processes of migration and accumulation of arsenic, which in turn depends on the processes of soil formation, including the expression of the eluvial process [67,68]. On the other hand, the close relationship with exchangeable magnesium cations, a correlation coefficient of 0.91 (Table 6), may indicate lateral differentiation.

Total concentrations of arsenic in soils are distributed mainly according to the regressive-accumulative type. Compared to the background concentrations of arsenic clarks in the upper part of the continental crust—4.8 mg/kg [69], in all the studied soils the concentrations of arsenic clarks in the upper mineral horizons exceed the background values by 3.7–5.2 times. Compared with background concentrations of rocks—6.49 mg/kg, which formed the studied soil (Table 7), the excess is on average 3 times and is characteristic only for the upper horizons of A. Compared with the standards of the maximum permissible concentration in the Russian federation—5.0 mg/kg [70], the excess is on average 3.5 times. The highest values were recorded in forest litter, which indicates the entry of arsenic into

soils by air mass transfer. Calculations of the bioconcentration coefficient (BCF) prove pollutant accumulation by plant litter [41]. The most intense impact of industrial air emissions occurs in the areas located on the top of the mountain range, where the maximum concentrations of arsenic (64.40 mg/kg) are recorded in the plant litter. Due to the lack of abundant vegetation and high forest at 824 m ASL, which act as barriers to arsenic migration, the main input occurs in the surface area. With decreasing altitude and downhill, arsenic concentrations in the forest floor noticeably decrease (Table 5). With a change in the type of vegetation to broad-leaved and almost complete absence of coniferous stands, the BCF coefficient decreases significantly and becomes less than 1 (Table 5).

Table 7. Statistical parameters *.

	n	M	Max	Min	σ	V	D
pH_{H2O}	16	4.94	5.60	3.95	0.41	8.38%	0.17
pH_{KCl}	16	3.76	4.06	3.26	0.22	5.76%	0.05
Ca^{2+}	21	5.06	13.65	1.32	3.49	68.93%	12.18
Mg^{2+}	21	3.95	12.76	0.57	3.78	95.68%	14.28
As in soil	21	17.13	64.40	2.81	16.06	93.73%	257.84
As in silt	11	6.49 **	12.56	2.81	3.15	48.47%	9.89

* Note: *n*–sample size, M—is the mean value of a statistical range, max and min—maximum and minimum values of the statistical range, σ—standard deviation, V—coefficient of variation, D—is the sample variance, **—background in soil, mg/kg.

The calculated values of arithmetic mean error and standard deviation (Table 7) indicate the reliability of the studies. High values of dispersion and variation for exchangeable calcium and magnesium cations, as well as for arsenic, indicate a wide dispersion of values. This is due to the accumulation of arsenic in the upper horizons of its intensive bioaccumulation by plants, against the background of low concentrations in the B and R horizons, which is reflected in the values of the maximum and minimum, as well as the mean values of the statistical series (Table 7).

4. Conclusions

The present studies of soils in mountain forest areas recorded high concentrations of arsenic that exceeded Clarke concentrations by 3.7–5.2 times in mineral horizons. When analyzing changes in arsenic concentrations in soils as altitude changes, it is discovered that the amount of pollutant decreases down the slope. The maximum concentrations of arsenic are found in the ground leaf litter, which indicates that the input of arsenic was mainly due to air mass transfer. A bioconcentration factor (BCF) greater than 1 proves the involvement of changes in arsenic concentrations in litter and soils.

Correlation analysis showed a close relationship between the content of the total content of arsenic in soils and exchangeable calcium and magnesium cations, as well as an inverse relationship with the increasing pH of the medium. Coefficients of variation and dispersion for the exchangeable cations of calcium, magnesium and arsenic indicate a high dispersion in concentrations between the upper soil horizons and parent rock, which may also indicate a constant delivery of arsenic with atmospheric flows.

Analysis of the mineralogical composition of silt and changes in arsenic concentrations in the silt fraction of soils suggests that this pollutant is mainly accumulated by secondary minerals of the clinochlore group. Neither minerals serving as a source of arsenic nor minerals of technogenic origin were found. The results obtained can serve as a guideline for monitoring the areas around the enterprise and provide a better understanding of pollutants' distribution in the soils of remote areas and mountain landscapes.

Author Contributions: Conceptualization, M.V.S. and M.S.M.; methodology, M.S.M.; validation, M.V.S., S.S.M. and D.G.N.; writing—original draft, M.V.S. and M.S.M.; writing—review & editing,

M.V.S., M.S.M., T.M.M. and S.S.M. All authors have read and agreed to the published version of the manuscript.

Funding: The study was supported by the grant from the Russian Science Foundation (project No. 21-77-20089) at the Southern Federal University.

Data Availability Statement: The data presented in this study are available on request from the corresponding author. The data are not publicly available due to privacy restrictions.

Conflicts of Interest: The authors declare no conflict of interest.

References

1. Pirrone, N.; Cinnirella, S.; Feng, X.; Finkelman, R.B.; Friedli, H.R.; Leaner, J.; Mason, R.; Mukherjee, A.B.; Stracher, G.B.; Streets, D.G.; et al. Global mercury emissions to the atmosphere from anthropogenic and natural sources. *Atmos. Chem. Phys.* **2010**, *10*, 5951–5964. https://doi.org/10.5194/acpd-10-4719-2010.
2. Tang, R.; Wang, H.; Luo, J.; Sun, S.; Gong, Y.; She, J.; Chen, Y.; Dandan, Y.; Zhou, J. Spatial distribution and temporal trends of mercury and arsenic in remote timberline coniferous forests, eastern of the Tibet Plateau, China. *Environ. Sci. Pollut. Res.* **2015**, *22*, 11658–11668. https://doi.org/10.1007/s11356-015-4441-7.
3. Beni, C.; Diana, G.; Marconi, S. Bovine milk chain in Italian farms. I. Arsenic levels in soil, gravitational and clean water, bovine diet, and milk. *Agrochimica* **2008**, *52*, 99–115.
4. Cui, J.-L.; Zhao, Y.-P.; Li, J.-S.; Beiyuan, J.-Z.; Tsang, D.C.; Poon, C.-S.; Chan, T.-S.; Wang, W.-X.; Li, X.-D. Speciation, mobilization, and bioaccessibility of arsenic in geogenic soil profile from Hong Kong. *Environ. Pollut.* **2018**, *232*, 375–384. https://doi.org/10.1016/j.envpol.2017.09.040.
5. Dong, H.; Lin, Z.; Wan, X.; Feng, L. Risk assessment for the mercury polluted site near a pesticide plant in Changsha, Hunan, China. *Chemosphere* **2017**, *169*, 333–341. https://doi.org/10.1016/j.chemosphere.2016.11.084.
6. Wang, X.; Bao, Z.; Lin, C.-J.; Yuan, W.; Feng, X. Assessment of Global Mercury Deposition through Litterfall. *Environ. Sci. Technol.* **2016**, *50*, 8548–8557. https://doi.org/10.1021/acs.est.5b06351.
7. Bing, H.; Zhou, J.; Wu, Y.; Luo, X.-S.; Xiang, Z.; Sun, H.; Wang, J.; Zhu, H. Barrier effects of remote high mountain on atmospheric metal transport in the eastern Tibetan Plateau. *Sci. Total Environ.* **2018**, *628–629*, 687–696. https://doi.org/10.1016/j.scitotenv.2018.02.035.
8. Tarvainen, T.; Reichel, S.; Müller, I.; Jordan, I.; Hube, D.; Eurola, M.; Loukola-Ruskeeniemi, K. Arsenic in agro-ecosystems under anthropogenic pressure in Germany and France compared to a geogenic As region in Finland. *J. Geochem. Explor.* **2020**, *217*, 106606. https://doi.org/10.1016/j.gexplo.2020.106606.
9. Ali, W.; Mao, K.; Zhang, H.; Junaid, M.; Xu, N.; Rasool, A.; Feng, X.; Yang, Z. Comprehensive review of the basic chemical behaviours, sources, processes, and endpoints of trace element contamination in paddy soil-rice systems in rice-growing countries. *J. Hazard. Mater.* **2020**, *397*, 122720. https://doi.org/10.1016/j.jhazmat.2020.122720.
10. Neal, C.; Robson, A.J. A summary of river water quality data collected within the Land-Ocean Interaction Study: Core data for eastern UK rivers draining to the North Sea. *Sci. Total Environ.* **2000**, *251–252*, 585–665. https://doi.org/10.1016/S0048-9697(00)00397-1.
11. Fernández-Caliani, J.C. Risk-based assessment of multimetallic soil pollution in the industrialized peri-urban area of Huelva, Spain. *Environ. Geochem. Health* **2012**, *34*, 123–139. https://doi.org/10.1007/s10653-011-9396-0.
12. Wang, S.; Mulligan, C.N. Occurrence of arsenic contamination in Canada: Sources, behavior and distribution. *Sci. Total Environ.* **2006**, *366*, 701–721. https://doi.org/10.1016/j.scitotenv.2005.09.005.
13. De Souza Neto, H.F.; da Silveira Pereira, W.V.; Dias, Y.N.; de Souza, E.S.; Teixeira, R.A.; de Lima, M.W.; Ramos, S.J.; do Amarante, C.B.; Fernandes, A.R. Environmental and human health risks of arsenic in gold mining areas in the eastern Amazon. *Environ. Pollut.* **2020**, *265*, 114969. https://doi.org/10.1016/j.envpol.2020.114969.
14. Huang, J.H. Impact of microorganisms on arsenic biogeochemistry: A review. *Water Air Soil Pollut.* **2014**, *225*, 1–25. https://doi.org/10.1007/s11270-013-1848-y.
15. Yamamura, S.; Amachi, S. Microbiology of inorganic arsenic: From metabolism to bioremediation. *J. Biosci. Bioeng.* **2014**, *118*, 1–9. https://doi.org/10.1016/j.jbiosc.2013.12.011.
16. Wenzel, W.W. Arsenic. In *Heavy Metals in Soils. Trace Metals and Metalloids in Soils and Their Bioavailability*, 3rd ed.; Alloway, B.J., Ed.; Springer: Berlin, Germany, 2013; pp. 241–282. https://doi.org/10.1016/S0003-2670(01)00924-2.
17. Campbell, K.M.; Nordstrom, D.K. Arsenic speciation and sorption in natural environments. *Rev. Mineral. Geochem.* **2014**, *79*, 185–216. https://doi.org/10.2138/rmg.2014.79.3.
18. Bolan, N.S.; Mahimairaja, S.; Kunhikrishnan, A.; Choppala, G. Phosphorus–arsenic interactions in variable-charge soils in relation to arsenic mobility and bioavailability. *Sci. Total Environ.* **2013**, *463*, 1154–1162. https://doi.org/10.1016/j.scitotenv.2013.04.016.

19. Arco-Lázaro, E.; Agudo, I.; Clemente, R.; Bernal, M. Arsenic (V) adsorption-desorption in agricultural and mine soils: Effects of organic matter addition and phosphate competition. *Environ. Pollut.* **2016**, *216*, 71–79. https://doi.org/10.1016/j.envpol.2016.05.054.
20. Lewińska, K.; Karczewska, A.; Siepak, M.; Szopka, K.; Gałka, B.; Iqbal, M. Effects of waterlogging on the solubility of antimony and arsenic in variously treated shooting range soils. *Appl. Geochem.* **2019**, *105*, 7–16. https://doi.org/10.1016/j.apgeochem.2019.04.005.
21. Linnik, V.G.; Bauer, T.V.; Minkina, T.M.; Mandzhieva, S.S.; Mazarji, M. Spatial distribution of heavy metals in soils of the flood plain of the Seversky Donets River (Russia) based on geostatistical methods. *Environ. Geochem. Health* **2022**, *44*, 319–333. https://doi.org/10.1007/s10653-020-00688-y.
22. Hechler, J.; Udachin, V.; Aminov, P.; Beckett, P.J.; Spiers, G.A. Efflorescent sulfate minerals of the Karabash mining/smelting area, Ural mountains, Russia. *Mineralogy* **2018**, *4*, 96–101.
23. Vodyanitskii, Y.; Minkina, T. Determination of the affinity of heavy metals to carrier phases in soils. *Environ. Geochem. Health* **2022**, *44*, 1277–1288. https://doi.org/10.1007/s10653-021-00938-7.
24. Sazykina, M.A.; Minkina, T.M.; Konstantinova, E.Y.; Khmelevtsova, L.E.; Azhogina, T.N.; Antonenko, E.M.; Karchava, S.K.; Klimova, M.V.; Sushkova, S.N.; Polienko, E.A.; et al. Pollution impact on microbial communities composition in natural and anthropogenically modified soils of Southern Russia. *Microbiol. Res.* **2022**, *254*, 126913. https://doi.org/10.1016/j.micres.2021.126913.
25. Vodyanitskii, Y.N.; Minkina, T.M.; Kubrin, S.P.; Linnik, V.G. Iron sulphides and their effect on the xrf measurement of the bulk chemical composition of badland soils near the karabash copper smelter, southern urals, Russia. *Geochem. Explor. Environ. Anal.* **2018**, *19*, 176–183. https://doi.org/10.1144/geochem2017-081.
26. Bauer, T.V.; Pinskii, D.L.; Minkina, T.M.; Shuvaeva, V.A.; Soldatov, A.V.; Mandzhieva, S.S.; Tsitsuashvili, V.S.; Nevidomskaya, D.G.; Semenkov, I.N. Application of XAFS and XRD methods for describing the copper and zinc adsorption characteristics in hydromorphic soils. *Environ. Geochem. Health* **2022**, *44*, 335–347. https://doi.org/10.1007/s10653-020-00773-2.
27. Minkina, T.M.; Linnik, V.G.; Nevidomskaya, D.G.; Bauer, T.V.; Mandzhieva, S.S.; Khoroshavin, V.Y. Forms of Cu (II), Zn (II), and Pb (II) compounds in technogenically transformed soils adjacent to the Karabash med copper smelter. *J. Soils Sediment* **2018**, *18*, 2217–2228. https://doi.org/10.1007/s11368-017-1708-2.
28. Gashkina, N.A.; Tatsii, Y.G.; Udachin, V.N.; Aminov, P.G. Biogeochemical indication of environmental contamination: A case study of a large copper smelter. *Geochem. Int.* **2015**, *53*, 253–264. https://doi.org/10.1134/S0016702915030076.
29. Weatherarchive.ru. Available online: http://weatherarchive.ru/Pogoda/Karabash (accessed on 14 February 2023).
30. *ISO 18400-104*; Soil quality—Sampling—Part 104. ISO: Geneva, Switzerland, 2018.
31. IUSS Working Group WRB. *World Reference Base for Soil Resources 2014, Update 2015. International Soil Classification System for Naming Soils and Creating Legends for Soil Maps*; Word Soil Resources Report, No 106; Food and Agriculture Organization: Rome, Italy, 2014; 181p.
32. *ISO 13317–2*; Determination of Particle Size Distribution by Gravitational Liquid Sedimentation Methods—Part 2: Fixed Pipette Method. ISO: Geneva, Switzerland, 2001.
33. *ISO 10390*; Soil Quality—Determination of pH. 2005.
34. *ISO 14235*; Soil Quality—Determination of Organic Carbon by Sulfochromic Oxidation. ISO: Geneva, Switzerland, 1998.
35. *ISO 23470*; Soil Quality—Determination of Effective Cation Exchange Capacity (CEC) and Exchangeable Cations. ISO: Geneva, Switzerland, 2011.
36. *ISO 14254*; Soil Quality—Determination of Exchangeable Acidity Using Barium Chloride Solution as Extractant. ISO: Geneva, Switzerland, 2018.
37. *ISO 14388-3*; Soil Quality—Acid-Base Accounting Procedure for Acid Sulfate Soils—Part 3: Suspension Peroxide Oxidation Combined Acidity and Sulfur (SPOCAS) Methodology. ISO: Geneva, Switzerland, 2014.
38. *ISO 20280*; Soil quality—Determination of Arsenic, Antimony and Selenium in Aqua Regia Soil Extracts with Electrothermal or Hydride-Generation Atomic Absorption Spectrometry. ISO: Geneva, Switzerland, 2007.
39. *ASTM D934-08*; Standard Practices for Identification of Crystalline Compounds in Water-Formed Deposits by X-ray Diffraction. ASTM: West Conshohocken, PA, USA, 2008.
40. Liu, B.; Ai, S.; Zhang, W.; Huang, D.; Zhang, Y. Assessment of the bioavailability, bioaccessibility and transfer of heavy metals in the soil-grain-human systems near a mining and smelting area in NW China. *Sci. Total Environ.* **2017**, *609*, 822–829. https://doi.org/10.1016/j.scitotenv.2017.07.215.
41. Wu, Y.; Wang, S.; Zhao, C.; Nan, Z.; Zhao, C. Ecological Safety and Spatial Distribution of Mercury and Arsenic in Qinghai Spruce Ecosystems in Remote Plateau Mountains, Northwest China. *Forests* **2022**, *13*, 1269. https://doi.org/10.3390/f13081269.
42. Schaller, M.; Ehlers, T-A. Vegetation and climate effects on soil production, chemical weathering, and physical erosion rates. *Preprint* **2021**. https://doi.org/10.5194/esurf-2021-22.
43. Drohan, P.J.; Raab, T.; Hirsch, F. Distribution of silty mantles in soils of the Northcentral Appalachians, USA. *Catena* **2020**, *194*, 104701. https://doi.org/10.1016/ j.catena.2020.104701.

44. Li, Q.; Wang, L.; Fu, Y.; Lin, D.; Hou, M.; Li, X.; Hu, D.; Wang, Z. Transformation of soil organic matter subjected to environmental disturbance and preservation of organic matter bound to soil minerals: A review. *J. Soils Sediments* **2023**, *23*, 1485–1500. https://doi.org/10.1007/s11368-022-03381-y.
45. Cirkel, D.G.; Witte, J.-P.; Bodegom, P.V. The influence of spatiotemporal variability and ad-aptations to hypoxia on empirical relationships between soil acidity and vegetation. *Eco-Hydrology* **2014**, *7*, 21–32. https://doi.org/10.1002/eco.1312.
46. Bhardwaj, K.; Singh, M.K.; Raj, D.; Verma, S.; Dahiya, G.; Sharma, S.K.; Sharma, M.K. Effect of Tree Leaf Litterfall on available Nutrients and Organic Carbon Pools of Soil. *Res. J. Sci. Technol.* **2022**, *14,* 226–232. https://doi.org/10.52711/2349-2988.2022.00037.
47. Rakhsh, F.; Golchin, A.; Al Agha, A.B.; Alamdari, P. Effects of exchangeable cations, mineralogy and clay content on the mineralization of plant residue carbon. *Geoderma* **2017**, *307*, 150–158. https://doi.org/10.1016/j.geoderma.2017.07.010.
48. Ritschel, T.; Aehnelt, M.; Totsche, K.U. Organic matter governs weathering rates and microstructure evolution during early pedogenesis. *Geoderma* **2023**, *429*, 116269. https://doi.org/10.1016/j.geoderma.2022.116269.
49. Sokolova, T.A. The role of soil biota in the weathering of minerals: A review of literature. *Eurasian Soil Sci.* **2011**, *44*, 56–72. https://doi.org/10.1134/S1064229311010121.
50. Sokolova, T.A.; Tolpeshta, I.I.; Topunova, I.V. Biotite weathering in podzolic soil under conditions of a model field experiment. *Eurasian Soil Sci.* **2010**, *43*, 1150–1158. https://doi.org/10.1134/S106422931010008X.
51. Sokolova, T.A. Decomposition of clay minerals in model experiments and in soils: Possible mechanisms, rates, and diagnostics (analysis of literature). *Eurasian Soil Sci.* **2013**, *46*, 91–105. https://doi.org/10.1134/S1064229313010080.
52. Lee, B.D.; Sears, S.K.; Graham, C.R.; Amrhein, C.; Vali, H. Secondary Mineral Genesis from Chlorite and Serpentine in an Ultramafic Soil Toposequence. *Soil Sci. Soc. Am. J.* **2003**, *67*, 1309–1317. https://doi.org/10.2136/sssaj2003.1309.
53. Joeckel, R.M.; Wally, K.D.; Clement, B.A.; Hanson, R.P.; Dillon, S.J.; Wilson, K.S. Secondary minerals from extrapedogenic per latus acidic weathering environments at geomorphic edges, Eastern Nebraska, USA. *Fuel Energy Abstr.* **2011**, *85*, 253–266. https://doi.org/10.1016/j.catena.2011.01.011.
54. Lyons, W.B.; Leslie, L.D.; Gooseff, M. Chemical Weathering in the McMurdo Dry Valleys, Antarctica. Hydrogeology, Chemical Weathering, and Soil Formation. *Hydrogeol. Chem. Weather. Soil Form.* **2021,** 205–216. https://doi.org/10.1002/9781119563952.ch11.
55. Owador, C.N.; Oboh, I.; Omiojieahior, F.A. Adsorption Isotherms for Naphthalene on Clay and Silt Soil Fractions: A Comparison of Linear and Nonlinear Methods. *Adv. Mater. Res.* **2011**, *367*, 359–364. https://doi.org/10.4028/www.scientific.net/AMR.367.359.
56. Williamson, B.J.; Udachin, V.; Purvis, O.W.; Spiro, B.; Cressey, G.; Jones, G.C. Characterisation of airborne particulate pollution in the Cu smelter and former mining town of Karabash, South Ural Mountains of Russia. *Environ. Monit. Assess*. **2004**, *98*, 235–259. https://doi.org/10.1023/b:emas.0000038189.45002.78.
57. Han, L.; Zhao, Y.; Hao, R. Arsenic emission and distribution characteristics in the ultra-low emission coal-fired power plant. *Environ. Sci. Pollut. Res.* **2022**, *29*, 36814–36823.. https://doi.org/10.1007/s11356-021-16745-7.
58. Matzen, S.; Fakra, S.; Nico, P.; Pallud, C. Pteris vittata Arsenic Accumulation Only Partially Explains Soil Arsenic Depletion during Field-Scale Phytoextraction. *Soil Syst.* **2020**, *4*, 71. https://doi.org/10.3390/soilsystems4040071.
59. Kwon, J.H.; Cho, J.S.; Lee, C.H. Effect of Arsenic Concentrations in Soil on Growth and Arsenic Accumulation of Pteris multifidi. *J. People Plants Environ.* **2015**, *18*, 273–280. https://doi.org/10.11628/ksppe.2015.18.4.273.
60. Demirayak, A.; Kutbay, G.; Surmen, B.; Kilic, D.D. Arsenic accumulation in some natural and exotic tree and shrub species in Samsun Provience (Turkey). *Anatol. J. Bot.* **2019**, *3*, 13–17. https://doi.org/10.30616/ajb.499141.
61. Frost, R.R. Effect of pH on adsorption of arsenic and selenium from landfill leachate by clay minerals. *Soil Sci. Soc. Am.* **1977**, *41*, 53–57.
62. Lindsay, W.L. *Chemical Equilibria in Soils*; John Wiley & Sons: New York, NY, USA, 1979; p. 449. https://doi.org/10.1346/CCMN.1980.0280411.
63. Sadiq, M. Arsenic chemistry in soils: An overview of thermodynamic predictions and field observations. *Water Air Soil Pollut.* **1997**, *93*, 117–136.
64. Karczewska, A.; Lewinska, K.; Siepak, M.; Galka, B.; Drabrach, A.; Szopka, K. Transformation of beech forest litter as a factor that triggers arsenic solubility in soils developed on historical mine dumps. *J. Soils Sediments* **2018**, *18*, 2749–2758. https://doi.org/10.1007/s11368-018-2031-2.
65. Qafoku, N.P.; Lawter, A.R.; Gillispie, E.C.; Elroy, E.M.; Smith, F.N.; Sahajpal, R.; Cantrell, K.; Freedman, V. Calcium carbonate minerals as scavengers of metals and radionuclides: Their role in natural attenuation and remediation. *Adv. Agron.* **2022**, *176*, 115–152. https://doi.org/10.1016/bs.agron.2022.07.003.
66. Gathuka, L.W.; Kasai, H.; Kato, T.; Takai, A.; Inui, T.; Katsumi, T. Evaluating the arsenic attenuation of soil amended with calcium–magnesium composites of different particle sizes. *Soils Found.* **2022**, *62*, 101130. https://doi.org/10.1016/j.sandf.2022.101130.
67. Mehmood, T., Ashraf, A., Peng, L., Shaz, M., Ahmad, S., Ahmad, S., Khan, I., Abid, M., Gaurav, G.K., Riaz, U. Modern Aspects of Phytoremediation of Arsenic-Contaminated Soils. In: Niazi, N.K., Bibi, I., Aftab, T. (eds) Global Arsenic Hazard. Environmental Science and Engineering. Springer Nature: Cham, Switzerland, 2023; Chapter 20; pp. 433–457. https://doi.org/10.1007/978-3-031-16360-9_20

68. Bei, Q.; Yang, T.; Ren, C.; Guan, E.; Dai, Y.; Shu, D.; He, W.; Tian, H.; Wei, G. Soil pH determines arsenic-related functional gene and bacterial diversity in natural forests on the Taibai Mountain. *Environ. Res.* **2023**, *220*, 15181. https://doi.org/10.1016/j.envres.2022.115181.
69. Rudnic, R.L.; Gao, S. *Composition of the Continental Crust. Treatise on Geo-Chemistry*; Elsevier: Amsterdam, The Netherlands, 2003; pp. 1–64. https://doi.org/10.1016/B978-0-08-095975-7.00301-6.
70. SANPIN (Sanitary Rules and Norms). *Hygienic Regulations and Requirements to Ensure Safety and (or) Harmlessness for Humans of Environmental Factors*; No. 1.2.3685-21; Federal Service for Supervision of Consumer Rights Protection and Human Welfare: Moscow, Russia, 2021. (In Russia).